

The influence of supporting ions on the electrochemical detection of individual silver nanoparticles: Understanding the shape and frequency of current transients in nano-impacts

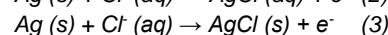
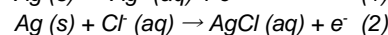
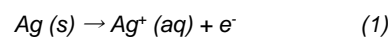
Kay J. Krause^[a], Fabian Brings^[a], Jan Schnitker^[a], Enno Kätelhön^[b], Philipp Rinklin^[c], Dirk Mayer^[a], Richard G. Compton^[b], Serge G. Lemay^[d], Andreas Offenhäusser^[a], and Bernhard Wolfrum^{*[a,c]}

Abstract: We report the influence of electrolyte composition and concentration on the stochastic amperometric detection of individual silver nanoparticles at microelectrode arrays and show that the sensor response at certain electrode potentials is dependent on both the conductivity of the electrolyte and the concentration of chloride ions. We further demonstrate that the chloride concentration in solution heavily influences the characteristic current spike shape of recorded nanoparticle impacts: While typically too short to be resolved in the measured current, the spike widths are significantly broadened at low chloride concentrations below 10 mM and range into the millisecond regime. The analysis of more than 25.000 spikes reveals that this effect can be explained by the diffusive mass transport of chloride ions to the nanoparticle, which limits the oxidation rate of individual silver nanoparticles to silver chloride at the chosen electrode potential.

Introduction

Silver nanoparticles are widely used for anti-microbial coatings^[1–4], sensing applications^[5–9], or as catalysts in electrochemical reactions^[10–15]. As a consequence, tons of nanoparticles are released every year either deliberately or accidentally into the environment. The quantification of silver nanoparticles raises interest concerning the spread and possible adverse side-effects on aqueous systems including fresh and saline waters^[16–19]. Amperometry at microelectrodes is capable of sensing individual particles in aqueous solution during nanoparticle impacts^[20,21]. An approach for the direct detection of silver nanoparticles is the

electrochemical oxidation at the surface of an appropriately biased electrode^[22–24]. Here, the charge transfer of electrons from the nanoparticle to the electrode is measured as a distinct spike in current-time traces. By counting the number of oxidation spikes per time information about the particle concentration is obtained^[25]. Furthermore, calculation of the total charge, which is transferred per spike, yields in principle information about the particle volume^[26–28] or surface area^[29]. For freely diffusing nanoparticles, the frequency of oxidation events is limited by the diffusive mass transport of particles to the electrode surface and therefore by the electrode size. However, the maximum electrode size is limited by the current noise, which makes the detection of small particles difficult by obscuring the oxidation spikes^[30]. To combine the advantages of low noise and high surface area, microelectrode arrays (MEAs) can be used^[31,32]. Nevertheless, accurate concentration measurements and particle sizing in arbitrary media are difficult as the oxidation of silver nanoparticles depends on different parameters including the electric field^[33], the electrolyte^[34–36], the electrode surface^[37–39] or the nanoparticle capping agent^[40]. In particular, nanoparticle detection is sensitive to the chloride concentration due to the possible oxidation of silver to silver chloride^[41]. It was previously shown that the oxidation of Ag nanoparticles may progress along various different reaction paths which include:



Equation 1-3. Different reaction pathways for the oxidation of silver.

A study^[41] by Toh et al. illustrated that in presence of chloride ions and depending on the chosen electrode potential either reaction (1) to Ag^+ or a reaction to AgCl along one or both of the reaction paths (2) and (3) prevails. Versus a home-built Ag/AgNO_3 reference electrode, the formation of Ag^+ was found between +50 and +250 mV (corresponding to approximately +530 and +730 mV vs. Ag/AgCl (3M KCl)), while the reaction to AgCl via reaction path (2) and/or (3) was observed between -300 and -200 mV (corresponding to approximately +180 and +280 mV vs. Ag/AgCl (3M KCl)). In the case of reaction path (1), the reaction rate may be either limited by the dissolution of silver or the solubility of silver ions in the solution adjacent to the nanoparticle. In comparison to reaction (1), the determination of the rate limiting process in reaction path (2) or (3) is, however more complicated as various processes may limit the reaction rate: The reaction of Ag to AgCl , the diffusion of Cl^- to the nanoparticle, the solubility of AgCl in the

- [a] K. J. Krause, F. Brings, J. Schnitker, Dr. D. Mayer, Prof. Dr. A. Offenhäusser, Prof. Dr. B. Wolfrum
Institute of Bioelectronics (PGI-8/ICS-8) and JARA—Fundamentals of Future Information Technology, Forschungszentrum Jülich, 52425 Jülich, Germany
E-Mail: bernhard.wolfrum@tum.de
- [b] Dr. E. Kätelhön, Prof. Dr. R. G. Compton
Department of Chemistry, Physical and Theoretical Chemistry Laboratory, Oxford University, South Parks Road, Oxford OX1 3QZ, United Kingdom
- [c] Dr. P. Rinklin, Prof. Dr. B. Wolfrum
Neuroelectronics, MSB, Department of Electrical and Computer Engineering, Technical University of Munich (TUM), Boltzmannstr. 11, 85748 Garching, Germany & Bernstein Center for Computational Neuroscience Munich
- [d] Prof. Dr. S. G. Lemay
MESA+ Institute for Nanotechnology, University of Twente, PO Box 217, 7500 AE Enschede, The Netherlands

Supporting information for this article is given via a link at the end of the document

FULL PAPER

immediate proximity of the nanoparticle in (2), or the diffusion of Cl^- through a shell of solid AgCl on the particle surface in (3) may be rate limiting. In addition, further reaction pathways may compete with the above that include the following reaction at high chloride ion concentrations:



Equation 4. Possible silver oxidation pathway at high chloride ion concentrations.

Independent of the electrode potential, the presence of oxygen may be another important factor in this context. A recent work^[42] on the fate of silver nanoparticles in aqueous solution by Plowman et al. showed that the reduction of O_2 drives the dissolution of silver nanoparticles while in the presence of chloride ions this dissolution is inhibited.

Here we investigate the oxidation of silver nanoparticles and its dependence on the chloride concentration in supporting electrolytes using microelectrode arrays. We show that at the investigated potentials the frequency of oxidation events depends on both the conductivity of the electrolyte and the absolute chloride concentration. Furthermore, we demonstrate that the shape of current transients generated by silver nanoparticle oxidation events can be described by an analytical model, which takes into account the chloride diffusion to a silver nanoparticle during oxidation as the rate-limiting reaction step.

Results and Discussion

We first investigate the impact frequency in current-time traces in the presence of nanoparticles at a different concentrations of supporting KCl electrolytes (Figure 1). Figures 1 b) and c) show representative recordings of the oxidation of silver nanoparticles from aqueous solution. The part of the current trace, which is plotted in red, is used to calculate the oxidation spike frequency. It is evident that the frequency of oxidation events, as well as the spike height, are highly dependent on the KCl concentration. Both the number of recorded events and the average spike amplitude are significantly decreased for a supporting electrolyte of 20 mM KCl compared to 55 mM KCl. In Figure 1 a) the average rate of particles being oxidized at a single electrode (frequency of oxidation events) is plotted against the KCl concentration for different oxidizing potentials applied vs. the Ag/AgCl reference electrode. For an applied potential below 300 mV the spike frequency increases with the potential at constant KCl concentration while the spike frequency becomes independent of the potential for a sufficiently high overpotential (300 to 500 mV). For a potential of 150 mV no oxidation events can be observed for KCl concentrations lower than 40 mM while for a potential of 200 mV even at 20 mM KCl oxidation events occur.

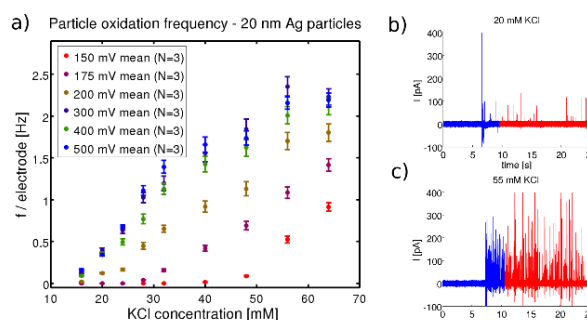


Figure 1. Frequency of nanoparticle oxidation events in aqueous solution for 12 μm MEAs at different potentials vs. Ag/AgCl reference electrode and different KCl concentrations (a). Current time traces for supporting electrolyte concentrations of 20 mM (b) and 55 mM (c). The large spike occurring after approximately seven seconds within the blue part of the current traces is related to particle insertion and only the red part of the current trace was used for data evaluation.

The trend in the data, showing a strong dependence of the nanoparticle impact frequency on the supporting electrolyte, can partly be explained by a shift in the oxidation potential. The formal potential for the oxidation of silver to silver chloride relative to the reference electrode (3 M KCl/Ag/AgCl) in a concentration Cl^- of m is given by Equation 5:

$$E_f^0 = \frac{RT}{F} \cdot \ln\left(\frac{a(m)}{a(3\text{ M})}\right) \quad (5)$$

Equation 5. The formal potential for the oxidation of silver to silver chloride. Here $a(m)$ is the activity of Cl^- in a concentration of m M Cl^- and $a(3\text{ M})$ is the activity of Cl^- in 3 M Cl^- . R is the universal gas constant, F is Faraday's constant and T the temperature.

The potential shift due to the concentration of chloride ions can hence be calculated to be ~ 110 mV for 40 mM KCl. However, this is only valid for a time-independent charge distribution within the electrochemical double layer. During electrochemical reactions at electrodes with nanometer scale, like the 20 nm silver nanoparticles used here, the electrochemical double layer is not at a steady state so the dynamics have to be taken into account. This leads to an additional potential drop at the point of electron transfer^[43]. Recent work^[44,45] further demonstrated that in nano-impacts Brownian motion of the analyte at the interface may lead to a modulation of the contact resistance and hence to additional fluctuations in the Faradaic current occur. If a sufficiently high overpotential is applied, in this case, more than 300 mV, each impact can be assumed to generate an oxidation event and the event rate becomes independent of the potential. For such oxidation potentials the spike frequency scales linearly with the chloride concentration in a concentration regime from 16 to 50 mM (0.25 to 0.75 S/m). A similar behavior was observed by Toh *et al.* using stripping voltammetry of deposited silver nanoparticles^[41]. At higher salt concentrations, the event frequency is limited by the diffusion of particles to the electrodes.

FULL PAPER

The dependence of the frequency on the KCl concentration can be explained by two mechanisms: an electrostatic effect, which occurs due to the low conductivity of the electrolyte or a depletion of chloride ions, which leads to insufficient oxidation reactions. To separate these possibilities we performed two different experiments: First, we measured the event frequency for an electrolyte with varying chloride content using a constant total amount of supporting salt. Here, the conductivity is approximately stable and we expect to recognize the particular influence of the chloride ions. Second, we measured the event rate at a constant chloride concentration with electrolytes of varying conductivity.

In Figure 2 the average frequency of oxidation events at a single electrode is shown for a constant electrolyte concentration of 80 mM (~1.2 S/m) with varying amounts of KCl and KNO₃. For KCl concentrations above 20 mM we observe a constant event frequency, which is limited by the diffusive mass transport of particles to the microelectrode. As shown previously, the net transport of particles to the electrode is affected by possible adsorption at the chip interface^[31]. However, below 20 mM, we see a strong decline of the event frequency with decreasing chloride concentration. This likely indicates that in the regime below 20 mM, the oxidation reaction is limited by the chloride flux to the silver nanoparticles.

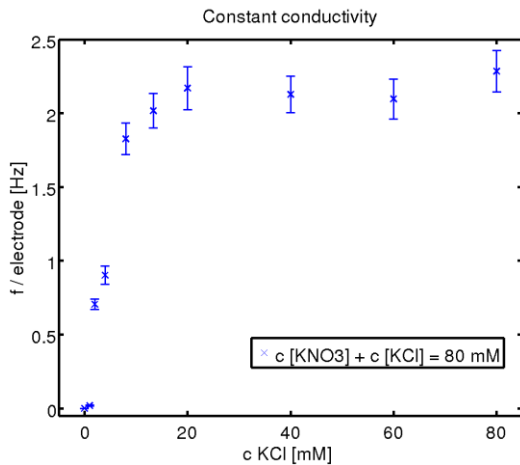


Figure 2. Frequency of nanoparticle oxidation events in aqueous solution for 12 μ m MEAs for a potential of 400 mV vs. a Ag/AgCl reference electrode and different electrolyte mixtures. The total amount of supporting salt for each measurement was 80 mM.

So far, we have only considered the effect of chloride ions on the frequency of recorded oxidation events, which is indicative of the concentration of silver nanoparticles. However, as the chloride concentration plays a dominant role, it can be expected that the shape of the recorded oxidation spikes is also influenced by the flux of chloride to the nanoparticle. These current transients can be described as the diffusion-limited flux to a sphere on a plate taking into account the shrinking radius of the sphere due to the consumption of material by the electrochemical reaction as described previously^[46].

$$I(t) = 4\pi l n(2) N_A e_0 D c_0 \cdot \sqrt{r_0^2 - \frac{2 \ln(2) N_A D c_0 m_{\text{atom}}}{\rho} \cdot t} \quad (6)$$

Equation 6. Time-dependend current transient for a nanoparticle oxidation limited by the diffusive mass transport of Cl⁻ to the oxidizing particle. Here N_A is the Avogadro constant, e_0 the elementary charge, $D = 2 \cdot 10^{-9} \frac{\text{m}^2}{\text{s}}$ the diffusion constant of Cl⁻, c_0 the bulk chloride concentration, $r_0 = 10 \text{ nm}$ the nanoparticle radius, m_A the atomic mass of silver and ρ the bulk density of silver.

It can be seen from Equation 6 that the expected spike height for $t = 0$ scales linearly with the chloride concentration and the nanoparticle radius. For a particle with a diameter of 20 nm the expected spike height is 17 pA for 1 mM Cl⁻, 34 pA for 2 mM Cl⁻, 68 pA for 4 mM Cl⁻ and 132 pA for 8 mM Cl⁻. Note that, in the experiment, the spike shape is influenced by the diffusion-limited chloride flux, the time a nanoparticle remains in proximity to the electrode, and the transfer function of the amplifier system. To address the effect of the diffusion-limited chloride flux, we have analyzed the spike shape as a function of the chloride concentration. In Figure 3, the current-time traces for different KCl concentrations are shown. The large spike within the blue part of the current trace is related to particle insertion and only the red part of the current trace was used for data evaluation. The observed oxidation spike height is of the same order of magnitude and scales linearly with the Cl⁻ concentration as per the analytical expectation. The variation within the measured spike heights is attributed to nanoparticles with sizes differing from 20 nm and particle agglomerations. In Figure 4 the mean shape of the measured oxidation spikes for 1 mM, 2 mM, 4 mM, 8 mM and 16 mM KCl is further shown (data points with error bars) together with predictions from the analytical model described by Equation 6. For comparison with the measured data, the analytical current transients are filtered with a 3 kHz fourth-order low-pass Bessel filter to mimic the amplifier bandwidth used in our experiments. The filter alters the analytical model in a way that smooth spike onsets and longer decay times are observed. Individual data sets are further time-shifted for clarity of presentation.

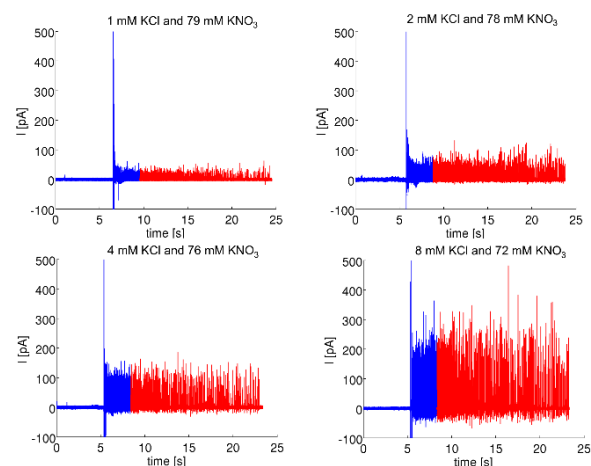


Figure 3. Measured current time traces for nanoparticle oxidation within different KCl concentrations. The total amount of salt (KCl+KNO₃) was 80 mM for each measurement. The large spike occurring after approximately five seconds within the blue part of the current traces is related to particle insertion and only the red part of the current trace was used for data evaluation.

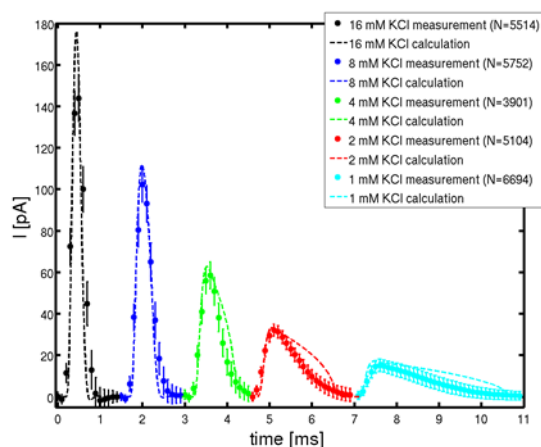


Figure 4. Comparison between the measured oxidation events for different chloride concentrations and the analytical calculation. The total salt concentration as the sum of KCl and KNO_3 was 80 mM for each measurement. The results from measurements obtained at different chloride concentrations are shifted in time for clarity of presentation. It is noted that the depicted theoretical model presents the result of Equation 6 digitally filtered via an emulation of the potentiostat's transfer function.

With increasing chloride concentration, the spike duration becomes smaller and the spike height increases as the larger chloride flux leads to a faster oxidation. It can be seen that the measured data closely matches the analytical results, indicating a diffusion-limited oxidation of the nanoparticle within the given chloride concentration range. For small concentrations of chloride and therefore long oxidation times, the tailing edge of the oxidation spike is overestimated by the analytical model, which assumes a complete oxidation of the nanoparticle. The overestimation might be caused by a hindered diffusive transport of chloride ions across the silver chloride shell of the partially oxidized particle if solid silver chloride is formed during the impact. Interestingly, even at very small KCl concentrations all particles are fully oxidized leading to a current transient that can be modeled via Equation 6. Yet, the question remains as to why the measured frequency of nanoparticle impacts decreases for KCl concentrations below 20 mM (Figure 2 b)). To answer this question we have to take a closer look at the employed data processing approach: The detection threshold for the automated spike detection algorithm is triggered above a minimal spike height of 40 pA. At low KCl concentrations the spike shape during nanoparticle impacts becomes smaller and wider (Figure 4). For a 20 nm particle and 2 mM KCl the spike current is expected to be 33 pA. As the maximum current scales also linearly with the particle radius, only large particles can be detected at low KCl concentrations. This behavior is shown in Figure 5, where the particle diameter is plotted for measurements in 2 mM KCl and 8 mM KCl. It can be seen that, for 2 mM KCl, particles smaller than 20 nm are underrepresented compared to the 8 mM KCl measurements. While the chloride concentration influences the detection for concentrations below 20 mM Cl^- , this does not

explain the linear dependence of the spike frequency on the KCl concentration as seen in Figure 1. To evaluate the influence of the conductivity of the electrolyte, we measured the nanoparticle oxidation frequency at a fixed KCl concentration of 20 mM while adding additional salt (KNO_3).

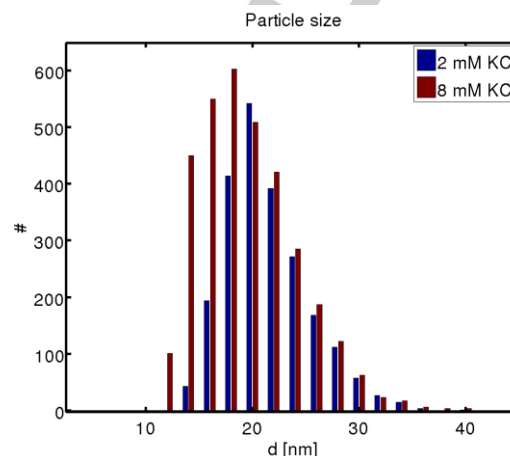


Figure 5. The size of Ag nanoparticles as derived from the total charge transferred per oxidation in 2 mM KCl and 8 mM KCl electrolyte.

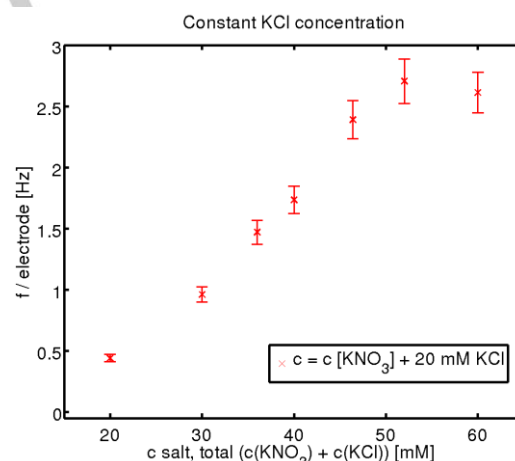


Figure 6. Nanoparticle oxidation frequency in aqueous solution for 12 μm MEAs for a potential of 400 mV vs. Ag/AgCl reference electrode and different KNO_3 concentrations. For each measurement the constant additional KCl concentration was 20 mM.

Figure 6 shows the oxidation frequency for a constant KCl concentration of 20 mM and additional KNO_3 , which feature a comparable molar conductivity. It can be seen that, for a total electrolyte concentration range from 20 to 50 mM (0.3 to 0.75 S/m), the spike frequency features the same linear behavior as in Figure 1 a), indicating that for this concentration range the detection is limited by the conductivity of the electrolyte^[33]. To further investigate this phenomenon, we compare the mean shape of all oxidation events from the measurements represented in Figure 6 with analytical calculations (see Figure 1, supporting material). The recorded spike shape mimics the analytical expectation for a salt concentration of 20 mM, independent of the

KNO_3 concentration but is effectively limited by the finite response time of the amplifier. The observed spike height is decreased for smaller KNO_3 concentrations. Therefore, both the spike height and the spike frequency depend on the conductivity of the electrolyte. One possible explanation for this behavior is the citrate shell of the silver nanoparticles, which stabilizes the particles by electrostatic repulsion. In pH 7 solutions with low electrolyte concentrations the nanoparticles feature a zeta potential of -40 mV, which represents the negative surface charge of the citrate shell^[47]. We however note a possible dependency of the particles' zeta potential on the chloride concentration: Ions may adsorb on the particle surface altering the surface potential and possibly stabilising the particles. In combination with steric effects, this citrate shell may influence the transport of negatively charged chloride ions to the silver surface. In addition, other effects including salt-dependent electrode modifications, electromigration^[48], the Frumkin effect^[49], a breakdown of electroneutrality^[50] and dynamic electrochemical double layer interactions^[43] may be of relevance in this context.

Conclusions

Current transients in the amperometric detection of oxidation events of individual silver nanoparticles to silver chloride in aqueous solution critically depend on the chloride concentration and can be modelled by an analytical equation taking into account the diffusion of chloride ions to the silver particle as the rate limiting step. The use of a microelectrode array enabled the collection of a significant amount of data for statistical analysis of the spike shapes and comparison to the theoretical model. In good agreement with theory, it was herein found that at low supporting Cl^- concentrations diffusion-limited mass transport leads to an increase in width and a decrease in amplitude of the recorded current transients. Reliable detection of nanoparticles therefore requires a minimal chloride concentration to avoid under-detection of nanoparticles. The amount of supporting chloride required depends on the background noise of the measurement system. As the detection of small spike amplitudes is limited by background noise, small particles cannot be detected at low chloride concentrations. Operating in the kHz range with a typical noise of approximately 1.5 pA (rms), a chloride concentration higher than 2 mM is needed to reliably detect silver nanoparticles with a size of 20 nm. In addition, the frequency of oxidation events depends linearly on the electrolyte conductivity for values between 0.3 and 0.75 S/m. These results provide parameters for the design of future sensing devices for robust and sensitive stochastic detection of nanoparticle concentration from aqueous solution. While in this work we specifically focused on the interactions of citrate-stabilized silver nanoparticles with chloride ions, similar effects can be expected to occur for other combinations of metal nanoparticles^[51,52], anions, and capping agents, which could be addressed in future studies.

Experimental Section

Microelectrode arrays were fabricated on $4''$ borosilicate wafers as substrate using standard cleanroom technology^[53]. The electrodes and feedlines were structured using photolithography and a lift-off process using a double-layer resist (nLof/LOR3B, MicroChemicals GmbH, Germany). A metal stack consisting of 10 nm titanium, 200 nm gold, and 10 nm titanium was deposited by electron-beam evaporation. The titanium served as adhesion layers between the gold and the substrate, as well as the gold and a passivation layer composed of an alternating layer of silicon oxide and silicon nitride with a total thickness of 800 nm. Each MEA features 64 electrodes, which are arranged in an 8×8 array with an inter-electrode distance of 200 μm . The diameter of the electrodes is 12 μm . Before use, the MEAs were cleaned by sonication in acetone for 5 min followed by sonication in isopropanol for 5 min and a final rinse with Milli-Q water (Millipore, 18.2 M Ω -cm). After each measurement, the MEAs were again rinsed with Milli-Q water. To establish a reservoir for the electrolyte solution, a glass ring with 15 mm diameter and 10 mm height was glued onto the MEA using polydimethylsiloxane (PDMS, Sylgard 184, Dow Corning, USA). As electrolyte, we used 700 μL of KCl and/or KNO_3 aqueous solutions. The citrate-stabilized silver nanoparticle dispersion was purchased from Sigma Aldrich, Germany. According to the product specifications it featured a silver concentration of 0.02 mg/mL and a particle diameter of 20 ± 4 nm as determined by transmission electron microscopy. The silver nanoparticle suspension was diluted with Milli-Q water directly before each measurement to a total particle concentration of 130 pM. 150 μL of silver nanoparticle solution is introduced into the aqueous solution (leading to a total particle concentration of 23 pM) approximately 7 seconds after the start of each measurement. Afterwards, two seconds of the current trace are neglected for data evaluation. The following 15 seconds of the current trace are then used to count the number of oxidation events (spikes) per time and electrode. The spike detection is performed using an automated algorithm written in Matlab, which selects spikes with a maximum amplitude that is larger than five times the root mean square of the baseline current. For the evaluation of the time-resolved oxidation current, a modified spike detection algorithm was used. To take into account elongated oxidation events with a lower maximum current in low chloride concentrations and to avoid a systematic change of the spike shape by overestimating the influence of noise events, the threshold criteria was set to a relative value that represents half of the expectation value. As reference an Ag/AgCl reference electrode was used (SuperDri-Ref SDR 2, World Precision Instruments, USA). The oxidation current was measured using a home-built amplifier system PicoAmp, which records all 64 independent channels simultaneously at a sampling frequency of 10 kHz per channel and an overall trans impedance gain of 10 mV/pA^[31,54].

Acknowledgements

We thank Marko Banzet and the Helmholtz Nanoelectronic Facility for the fabrication of microelectrode arrays, Norbert Wolters for the development of the electronic amplifier system, and Kristina Tschulik and Christopher Batchelor-McAuley for helpful discussions. We gratefully acknowledge funding by the Helmholtz Young Investigators Program and from the European Research Council under the European Union Seventh Framework Programme (FP/2007-2013)/ERC Grant Agreement no. [320403].

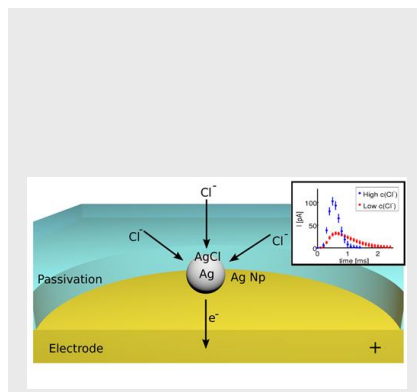
Keywords: Electrochemistry • Nanoparticles • Silver • Oxidation

- [1] J. R. Morones, J. L. Elechiguerra, A. Camacho, K. Holt, J. B. Kouri, J. T. Ramírez, M. J. Yacaman, *Nanotechnology* **2005**, *16*, 2346.

- [2] O. Choi, K. K. Deng, N.-J. Kim, L. Ross Jr., R. Y. Surampalli, Z. Hu, *Water Res.* **2008**, *42*, 3066–3074.
- [3] V. K. Sharma, R. A. Yngard, Y. Lin, *Adv. Colloid Interface Sci.* **2009**, *145*, 83–96.
- [4] M. Ahamed, M. S. AlSalhi, M. K. J. Siddiqui, *Clin. Chim. Acta* **2010**, *411*, 1841–1848.
- [5] X. Luo, A. Morrin, A. J. Killard, M. R. Smyth, *Electroanalysis* **2006**, *18*, 319–326.
- [6] J. Klein, *Proc. Natl. Acad. Sci.* **2007**, *104*, 2029–2030.
- [7] J. Zhang, B. P. Ting, N. R. Jana, Z. Gao, J. Y. Ying, *Small* **2009**, *5*, 1414–1417.
- [8] W. Song, H. Li, H. Liang, W. Qiang, D. Xu, *Anal. Chem.* **2014**, *86*, 2775–2783.
- [9] J. C. Cunningham, M. R. Kogan, Y.-J. Tsai, L. Luo, I. Richards, R. M. Crooks, *ACS Sens.* **2015**, DOI 10.1021/acssensors.5b00051.
- [10] R. Xu, D. Wang, J. Zhang, Y. Li, *Chem. – Asian J.* **2006**, *1*, 888–893.
- [11] J.-N. Chazalviel, P. Allongue, *J. Am. Chem. Soc.* **2011**, *133*, 762–764.
- [12] E. J. E. Stuart, N. V. Rees, R. G. Compton, *Chem. Phys. Lett.* **2012**, *531*, 94–97.
- [13] C. C. M. Neumann, E. Laborda, K. Tschulik, K. R. Ward, R. G. Compton, *Nano Res.* **2015**, DOI 10.1021/acssensors.5b00051.
- [14] V. K. Vidhu, D. Philip, *Micron* **2014**, *56*, 54–62.
- [15] C. M. Hill, J. Kim, A. J. Bard, *J. Am. Chem. Soc.* **2015**, *137*, 11321–11326.
- [16] T. M. Benn, P. Westerhoff, *Environ. Sci. Technol.* **2008**, *42*, 4133–4139.
- [17] A. G. Howard, *J. Environ. Monit.* **2010**, *12*, 135–142.
- [18] S. Klitzke, G. Metreveli, A. Peters, G. E. Schaumann, F. Lang, *Sci. Total Environ.* **2015**, *535*, 54–60.
- [19] L. Li, M. Stoiber, A. Wimmer, Z. Xu, C. Lindenblatt, B. Helmreich, M. Schuster, *Environ. Sci. Technol.* **2016**, *50*, 6327–6333.
- [20] B. M. Quinn, P. G. van't Hof, S. G. Lemay, *J. Am. Chem. Soc.* **2004**, *126*, 8360–8361.
- [21] X. Xiao, A. J. Bard, *J. Am. Chem. Soc.* **2007**, *129*, 9610–9612.
- [22] Y.-G. Zhou, N. V. Rees, R. G. Compton, *Angew. Chem. Int. Ed.* **2011**, *50*, 4219–4221.
- [23] E. J. E. Stuart, N. V. Rees, J. T. Cullen, R. G. Compton, *Nanoscale* **2012**, *5*, 174–177.
- [24] M. Z. M. Nasir, M. Pumera, *Phys. Chem. Chem. Phys.* **2016**, *18*, 28183–28188.
- [25] E. J. E. Stuart, Y.-G. Zhou, N. V. Rees, R. G. Compton, *RSC Adv.* **2012**, *2*, 6879–6884.
- [26] J. Ellison, K. Tschulik, E. J. E. Stuart, K. Jurkschat, D. Omanović, M. Uhlemann, A. Crossley, R. G. Compton, *ChemistryOpen* **2013**, *2*, 69–75.
- [27] W. Cheng, R. G. Compton, *TrAC Trends Anal. Chem.* **2014**, *58*, 79–89.
- [28] M. Pumera, *ACS Nano* **2014**, *8*, 7555–7558.
- [29] C. L. Bentley, M. Kang, P. R. Unwin, *J. Am. Chem. Soc.* **2016**, DOI 10.1021/jacs.6b08124.
- [30] J. Ellison, C. Batchelor-McAuley, K. Tschulik, R. G. Compton, *Sens. Actuators B Chem.* **2014**, *200*, 47–52.
- [31] K. J. Krause, A. Yakushenko, B. Wolfrum, *Anal. Chem.* **2015**, *87*, 7321–7325.
- [32] S. V. Sokolov, C. Batchelor-McAuley, K. Tschulik, S. Fletcher, R. G. Compton, *Chem. – Eur. J.* **2015**, *21*, 10741–10746.
- [33] K. Tschulik, W. Cheng, C. Batchelor-McAuley, S. Murphy, D. Omanović, R. G. Compton, *ChemElectroChem* **2015**, *2*, 112–118.
- [34] J. C. Lees, J. Ellison, C. Batchelor-McAuley, K. Tschulik, C. Damm, D. Omanović, R. G. Compton, *ChemPhysChem* **2013**, *14*, 3895–3897.
- [35] W. Cheng, E. J. E. Stuart, K. Tschulik, J. T. Cullen, R. G. Compton, *Nanotechnology* **2013**, *24*, 505501.
- [36] E. J. E. Stuart, K. Tschulik, D. Omanović, J. T. Cullen, K. Jurkschat, A. Crossley, R. G. Compton, *Nanotechnology* **2013**, *24*, 444002.
- [37] S. E. F. Kleijn, S. C. S. Lai, M. T. M. Koper, P. R. Unwin, *Angew. Chem. Int. Ed.* **2014**, *53*, 3558–3586.
- [38] C.-H. Chen, E. R. Ravenhill, D. Momotenko, Y.-R. Kim, S. C. S. Lai, P. R. Unwin, *Langmuir* **2015**, *31*, 11932–11942.
- [39] K. J. Krause, N. Adly, A. Yakushenko, J. Schnitker, D. Mayer, A. Offenhäusser, B. Wolfrum, *Anal. Chem.* **2016**, *88*, 3632–3637.
- [40] H. S. Toh, K. Jurkschat, R. G. Compton, *Chem. – Eur. J.* **2015**, *21*, 2998–3004.
- [41] H. S. Toh, C. Batchelor-McAuley, K. Tschulik, R. G. Compton, *Analyst* **2013**, *138*, 4292–4297.
- [42] B. J. Plowman, K. Tschulik, E. Walport, N. P. Young, R. G. Compton, *Nanoscale* **2015**, *7*, 12361–12364.
- [43] R. He, S. Chen, F. Yang, B. Wu, *J. Phys. Chem. B* **2006**, *110*, 3262–3270.
- [44] X. Li, C. Batchelor-McAuley, S. A. I. Whitby, K. Tschulik, L. Shao, R. G. Compton, *Angew. Chem. Int. Ed.* **2016**, *55*, 4296–4299.
- [45] H. Hodson, X. Li, C. Batchelor-McAuley, L. Shao, R. G. Compton, *J. Phys. Chem. C* **2016**, *120*, 6281–6286.
- [46] E. Kätelhön, E. E. L. Tanner, C. Batchelor-McAuley, R. G. Compton, *Electrochimica Acta* **2016**, *199*, 297–304.
- [47] A. M. E. Badawy, T. P. Luxton, R. G. Silva, K. G. Scheckel, M. T. Suidan, T. M. Tolaymat, *Environ. Sci. Technol.* **2010**, *44*, 1260–1266.
- [48] S. Chen, A. Kucernak, *J. Phys. Chem. B* **2002**, *106*, 9396–9404.
- [49] S. M. Oja, M. Wood, B. Zhang, *Anal. Chem.* **2013**, *85*, 473–486.
- [50] C. P. Smith, H. S. White, *Anal. Chem.* **1993**, *65*, 3343–3353.
- [51] B. Haddou, N. V. Rees, R. G. Compton, *Phys. Chem. Chem. Phys.* **2012**, *14*, 13612–13617.
- [52] M. Giovanni, A. Ambrosi, Z. Sofer, M. Pumera, *Electrochem. Commun.* **2015**, *56*, 16–19.
- [53] A. Yakushenko, V. Schöps, D. Mayer, A. Offenhäusser, B. Wolfrum, *Phys. Status Solidi A* **2014**, *211*, 1364–1371.
- [54] A. Yakushenko, E. Kätelhön, B. Wolfrum, *Anal. Chem.* **2013**, *85*, 5483–5490.

FULL PAPER

We report the influence of electrolyte composition and concentration on the stochastic amperometric detection of individual silver nanoparticles. While typically too short to be resolved in the measured current, the spike widths are significantly broadened at small chloride concentrations below 10 mM. The analysis of more than 25,000 spikes reveals that this effect can be explained by the diffusive mass transport of chloride ions to the nanoparticle.



Kay J. Krause, Fabian Brings, Jan Schnitker, Enno Kätelhön, Dirk Mayer, Richard G. Compton, Serge G. Lemay, Andreas Offenhäusser, and Bernhard Wolfrum*

Page No. – Page No.

The influence of supporting ions on the electrochemical detection of individual silver nanoparticles: Understanding the shape and frequency of current transients in nano-impacts